Ventral-aspect radar cross sections and polarization patterns of insects at X band and their relation to size and form

V. A. Drake[ab], J. W. Chapman[c], K. S. Lim[d], D. R. Reynolds[ed], J. R. Riley[de1], and A. D. Smith[de1]

[a]School of Physical, Environmental and Mathematical Sciences, UNSW Canberra, The University of New South Wales, Canberra, Australia; [b]Institute for Applied Ecology, University of Canberra, Canberra, Australia; [c]Centre for Ecology and Conservation, and Environment and Sustainability Unit, University of Exeter, Penryn, UK; [d]Department of AgroEcology, Rothamsted Research, Harpenden, UK; [e]Natural Resources Institute, University of Greenwich, Chatham, UK.

Author for correspondence: V. A. Drake, School of PEMS, UNSW Canberra, PO Box 7916, Canberra BC 2610, Australia; email a.drake@adfa.edu.au; fax +61-(0)2-62688786; tel and SMS +61-(0)409-651-257.

Other author contact information: JWC +44-(0)1326-371892 J.Chapman2@exeter.ac.uk Centre for Ecology and Conservation, University of Exeter, Penryn Campus, Penryn, Cornwall, TR10 9FE, UK; KSL +44-(0)1582-938677 jason.lim@rothamsted.ac.uk AgroEcology Dept., Rothamsted Research, Harpenden, Herts, AL5 2JQ, UK; DRR +44-(0)1634-883223 D.Reynolds@greenwich.ac.uk Natural Resources Institute, University of Greenwich, Central Avenue, Chatham Maritime, Kent, ME4 4TB, UK; JRR +44-(0)-1684-562777 joseph_riley@tiscali.co.uk 68 Peachfield Road, Malvern, Worcs, WR14 4AL, UK; ADS +44-(0)-1684-573705 alansmithsite@sky.com 41 Broadlands Drive, Malvern, Worcs, WR14 1PW, UK.

Disclosure statement. The authors declare that they have no financial interest in the application of this research.

ORCID   V. A. Drake − 0000-0001-9031-7906.

            J. W. Chapman − 0000-0002-7475-4441.

D. R. Reynolds – 0000-0001-8749-7491.

K.S. Lim – 0000-0002-9166-2928.

Footnote

[1]Retired.

[Note on supplemental files. These two files are Excel workbooks (.xlsx, 59 and 19 kB) each with a single sheet containing a table of data and associated notes.]

Ventral-aspect radar cross-sections and polarization patterns of insects at X band and their relation to size and form

ABSTRACT

A dataset of ventral-aspect insect radar cross-sections (RCSs) and polarization patterns, measured at X band (9.4 GHz, linear polarization) in laboratory rigs, has been collated from a number of sources. The data have been analysed to identify relationships between RCS parameters (one representing size and two the polarization-pattern shape) and the insects' masses and morphological dimensions and forms. An improved mass-estimation relationship, with appropriate asymptotes for very small and very large insects, is presented. This relationship draws only on the RCS size parameter and it is shown that incorporating one or both of the RCS shape parameters provides little additional benefit. Small insects have polarization-pattern shapes that fall within a relatively limited region of the range of parameter values allowed by electromagnetic scattering theory. Larger insects have shapes that extend beyond this region, following a broad trajectory as size and mass increases; at masses above ~0.6 g the pattern becomes 'perpendicular', with maxima when the E-field is orthogonal to the body axis rather than parallel to it. RCS shape can be used to infer morphological form for small insects (<80 mg), but not for larger ones. These results are consistent with observations from X-band vertical-beam entomological radars and provide a basis for identification, at least to broad taxon classes, of the targets detected by such radars.

Keywords: insect; radar cross-section; polarization pattern; mass estimation; morphological form

1.   Introduction

A variety of radar types have proved to be effective at detecting insects in flight,

especially when the insects have risen above terrain features and vegetation (Drake and

Reynolds 2012). Flights at these higher altitudes usually constitute migrations (Dingle

2014) and may lead to invasions of growing crops and consequent economic losses

(Drake and Gatehouse 1995; Koul, Cuperus, and Elliott 2008). Radar provides the only

practical means of acquiring information about such flights (e.g. Chapman, Reynolds, et

al. 2002; Chapman et al. 2005, 2006; Drake and Reynolds 2012, chapters 12, 13; Drake

and Wang 2013). In addition, radar observation has proved critical to recent research

into the cues that insects use to determine their orientation (heading direction) while

flying hundreds of metres above the surface, often in darkness, and into the effects these

orientation behaviours have on the insects' flight trajectories (Chapman et al. 2010; Hu,

Lim, Reynolds, et al. 2016; Reynolds et al. 2016).

A radar configuration that has proved particularly useful for observing insect

migrations employs a vertical beam that incorporates both rotating linear polarization

and a very narrow angle conical scan (Chapman, Smith, et al. 2002; Drake 2002). With

this 'ZLC configuration' (also known as a 'VLR' or *vertical-looking radar*), insects are

interrogated by the beam modulations during the few seconds that it takes for them to

complete a beam transit. Analysis of the rather complicated echo signal time series

allows retrieval of information not only about the individual insect's trajectory (its

height, its speed and direction of movement, and its heading direction) but also about its

identity. The latter takes the form of four parameters characterising the target: one

measure of size, two of shape, and the wing-beat frequency (though for some echoes no

wing-beating is detectable). Some or all of these parameters have been used to

discriminate target types and, in association with other data (e.g. trap catches), make

identifications of the species undertaking the migrations (e.g. Chapman, Reynolds, et al.

2002; Chapman et al., 2005, 2006, 2010; Drake and Wang 2013). A study of a large

sample of echoes for which all four parameters were retrieved, obtained over eight

months from a single site in inland eastern Australia using an X-band ZLC radar,

revealed several distinct target classes which occurred with varying frequency from

night to night and from month to month (Drake 2016).

From the viewpoint of a biologist user, mass is a much more readily

interpretable measure of target size than any directly radar-observable quantity. It is the

most obvious identification character to use when relating radar observations of

airborne insects to samples obtained from aerial or ground-level traps, in part because

the range of insect masses is very large (>4 orders of magnitude). Mass values also feed

directly into estimates of 'bioflow' and consideration of aero-ecological processes (Isard

and Gage 2001; Frick et al. 2013; Hu, Lim, Horvitz, et al. 2016), so their estimation has

intrinsic biological value. Methods for estimating the masses of insect targets from their

radar properties, especially the *radar cross section* (RCS, the radar measure of target

size), have been developed previously and are considered again here. It would

obviously be useful if further quantities could be identified that would allow

discrimination between targets with similar masses; these would constitute information

dimensions orthogonal to that provided by the measure of radar size. The obvious

candidates for such quantities are the wing-beat frequency (see below) and the two

shape parameters, either singly or in combination. Because the radar wavelength is

comparable to the size of the insect targets, the shape parameters can be expected to

provide information only about large-scale features. The obvious candidate is the

length:width ratio, termed here the 'form' $f = l/w$. The primary aim of this study has been

to identify relationships linking the three radar-target parameters to m and f, and if these

are informative to develop equations for routine estimation of these two characters from

ZLC-radar observation data.

Association of target properties with RCS size and shape values can be achieved

through calculation using electromagnetics theory or by measurement. Application of

theory to biological targets presents many challenges and so far has been confined to a

single example (a bat; Mirkovic et al., 2016). Laboratory measurements of the RCSs of

insects for which the species identification is known have been made on several

occasions (summarized in Drake and Reynolds 2012, chapter 4). For this paper we have

compiled a dataset containing all available vertical-incidence measurements made at X-

band frequencies (~9.4 GHz) for which both size and shape parameters were obtained;

we have then used this empirical data to examine the relationships between the masses

and morphological properties of insects and their observable radar properties.

Associations between radar parameters and taxonomic group will also be searched for.

Some of the values in the dataset are from published research, some are from archived

data for which only selected results had been published previously, and some are new

measurements.

The fourth identification parameter retrievable from ZLC echoes, the wing-beat

frequency, may also have utility both for inferring target mass (as larger insects

generally have lower wing-beat frequencies; Dudley 2000, chapter 3) and as an

orthogonal dimension for discriminating between targets of similar masses (Drake

2016). However, it was not determined for the specimens measured and is not

considered further in this report.

2.   Parameters, datasets, and measurements

2.1.   *Size, shape, and the polarization pattern*

Both the ZLC observations and the laboratory measurements determine the

backscattering RCS of a single insect oriented with its underside directed towards the

beam ('ventral aspect'), and the variation of this with polarization angle (i.e. with the

direction of the electric field of a linear-polarized electromagnetic wave). The variation of the RCS with polarization angle is termed the 'copolar linear polarization pattern' (CLPP). In the case of the laboratory measurements, the specimen was mounted horizontally and upright with the underside down, in the expectation that this approximates a normal flight attitude, and the beam was directed vertically. The zero angle of the CLPP is defined to be aligned with the main axis of the insect's body. For the radar observations, it is not certain that the targets have adopted an upright and horizontal attitude (see below), so it should only be said that the RCS values relate to zenith incidence.

A generally steady flight is to be expected during migration, and an absence of manoeuvring during the beam transit is assumed in the analysis of the echo-signal time series. This assumption is essentially validated whenever a good quality fit to an echo signal is obtained, as required for successful retrieval of the flight and target-identification parameters (Drake and Reynolds 2012, pp. 156-159). A steady flight suggests an upright stance (i.e. zero roll angle) but it does not require the insect's body to be horizontal and there is now evidence that some migrating insects (particularly small ones) fly with a non-zero (and positive, i.e. head above tail) pitch angle (Melnikov, Istok, and Westbrook 2015). The effect of a pitched attitude cannot be explored with the dataset available for this study and is not considered further, except to note that: (1) consideration of electromagnetic scattering processes suggests pitch effects will be slight if the pitch is only moderate, at least for targets that are not much longer than a wavelength (32 mm for the X band radars of concern here); and (2) radar-observed CLPPs (Dean and Drake 2005) appear compatible with the laboratory measurements reported here.

For copolar-linear observations, the variation of the RCS σ with polarization angle ϕ has the general form

$$\sigma(\phi) = a_0[1 + \alpha_2\cos2(\phi - \theta_2) + \alpha_4\cos4(\phi - \theta_4)] , \qquad (1)$$

where a_0 is the zenith-incidence polarization-averaged RCS and α_2 and α_4 are dimensionless parameters with positive values (Aldhous 1989; Dean and Drake 2005). The parameter a_0 is a measure of the target's size, with dimensions L^2 (i.e. area; units m^2 or, more commonly for insect targets, cm^2; often expressed logarithmically as decibels relative to 1 cm^2, denoted dBsc). In comparison with RCSs provided by other radar configurations, a_0 has the considerable advantage of relating to a consistent aspect and of being independent of the insect's orientation. Relationships between a_0 and mass have been developed previously (Aldhous 1989; Chapman, Smith, et al. 2002; Wang 2008); an improved relationship incorporating the additional data available to this study is presented here.

The expression in square brackets in Equation (1) is the CLPP. For a bilaterally symmetric target, which an insect in unbanked flight will constitute to a good approximation, the CLPP must also exhibit bilateral symmetry and therefore θ_2 and θ_4 must be equal. Symmetry considerations also require that the common value, denoted θ_0, must represent either the target's body axis or the perpendicular to it. Both radar observations (e.g. Dean and Drake 2005) and laboratory measurements (Hobbs and Aldhous 2006) are generally consistent with a common value for θ_2 and θ_4, and this simpler CLPP form has been used in the analyses presented here. The α_2 term in the CLPP produces elongation (of a basic circular form) and α_4 contributes a cruciform element. Consideration of electromagnetic scattering mechanisms indicates that for insects that are small relative to a wavelength the elongation direction of the CLPP will coincide with the body axis. Previous analyses of measurements at X band have

confirmed this and have also demonstrated that for very large insects (e.g. female

migratory locusts *Locusta migratoria*, typical mass ~3 g) CLPP elongation occurs at

right angles to the body axis (Riley 1985). Following Dean and Drake (2005), these two

CLPP types will be referred to as 'parallel' and 'perpendicular' respectively. For the

measurements, the insects were oriented in the rig with their heads towards $\theta_0 = 0$. For

observations made with a radar, determining whether θ_0 represents the body axis or the

normal to it requires additional, *a priori*, information (such as that the observations are

being made in a region where the aerial fauna includes very few large insects). Even if

the 90° uncertainty is resolved, ambiguity about whether the heading direction is θ_0 or

$\theta_0 + 180°$ (for the parallel case) will remain.

According to electromagnetic theory, the parameters α_2 and α_4 are positive and

are constrained by

$$\alpha_4 \leq \left(1 \pm \sqrt{1 - \alpha_2^2/2}\right)/2 \qquad (2)$$

(Dean and Drake 2005). This equation defines a semi-elliptical boundary with

$0 \leq \alpha_2 \leq \sqrt{2}$ and $0 \leq \alpha_4 \leq 1$, the ellipse centre being at $(\alpha_2, \alpha_4) = (0, \frac{1}{2})$. In the

measurement data, the angle θ_0 for targets with perpendicular CLPPs will be retrieved

as ~90°. An alternative scheme for representing perpendicular targets is to retain θ_0 as

representing the body axis (i.e. $\theta_0 = 0$), but to make α_2 negative (Dean 2007); this

moves these shapes into the left-hand half of the constraint ellipse so that they are

clearly separated from similarly-shaped CLPPs with parallel alignment. This reset is

straightforward for the laboratory measurements, for which the true alignment is known,

and is adopted in this work. It is of course problematic for observation data unless some

means of distinguishing the parallel and perpendicular cases is available.

Various transformations or combinations of the variables a_0, α_2, α_4 and θ_0 are available and some have interpretative value in particular circumstances (Aldhous 1989; Hobbs and Aldhous 2006; Dean 2007; Drake 2016). The 'harmonic model' (Hobbs and Aldhous 2006) of Equation (1) appears natural and straightforward and has been used in a previous investigation of insect target shapes (Dean and Drake 2005); it will form the basis for the present analysis. There will however be some discussion of the parallel $\sigma_{xx} = \sigma(\phi - \theta_0 = 0)$ and transverse $\sigma_{yy} = \sigma(\phi - \theta_0 = 90°)$ RCS values, which can be obtained from the transformations (Aldhous 1989, p. 21)

$$\sigma_{xx} = a_0(1 + \alpha_2 + \alpha_4) \tag{3a}$$

$$\sigma_{yy} = a_0(1 - \alpha_2 + \alpha_4) \ . \tag{3b}$$

The ratio of these two RCSs, $r_{sh} = \sigma_{xx}/\sigma_{yy}$, contours of which form straight lines in the (α_2, α_4) plane, will receive particular attention. Use will also be made of the orthogonal variables (p, q) introduced by Drake (2016). Contours of p are concentric ellipses, with $p = 1$ defining the constraint boundary of Equation (2) and $p = 0$ the central point at $(\alpha_2, \alpha_4) = (0, 0.5)$. Contours of q are orthogonal to these and form curves that run from the centre to the periphery, with $q = 0$ coincident with the α_4 axis, $q = 1$ intersecting the boundary at $\alpha_2 \approx 0.9$, and $q = 2$ intersecting at $\alpha_2 \approx 1.4$, just below the boundary's right-hand maximum. The (p, q) system becomes unsatisfactory for $\alpha_4 \geq 0.5$, but such targets occur infrequently and there is only one example in the measurement dataset.

2.2. The dataset and data sources

The CLPP data used in this analysis comprise 156 specimens of 40 species (Table 1). They originate from four sources: (1) measurements made in 1979 by JRR and associates at the Centre for Overseas Pest Research, U.K., denoted here by C; (2) measurements by Aldhous (1989), denoted A; (3) measurements by Wolf et al. (1993),

denoted W; and (4) measurements made in 2006 by ADS and DRR at Rothamsted

Research, U.K., denoted S. The species included are mainly grasshoppers and locusts

(Orthoptera) and moths and butterflies (Lepidoptera), two groups that include numerous

migratory species (Johnson 1969); a few beetles (Coleoptera), bees and wasps

(Hymenoptera), and craneflies (Diptera) are also present. All specimens occur once only

in the dataset. There are five species for which measurements are available from two

sources and 11 species for which measurements of five or more specimens are

available; however, intra-specific variation is not considered in this paper.

The specimens derive from Europe (southern England, C, A, S) and North

America (USA, W), or from laboratory cultures of African and North American species

(C, A, and probably W). Many of the species measured are known migrants and some

have been the subject of entomological radar observations (Drake and Reynolds 2012,

chapters 10-13). A few probably non-migratory species appear to have been included

because of their ready availability when measurements were being made; these add

diversity to the sample and in some cases provide examples of particular body forms

and sizes. Most of the species represented occur only in one continent and the dataset

will therefore not be representative of the migrating insect fauna at any actual ZLC-

radar observing site. This is especially the case for the orthopteran subsample, which

comprises only six species of which four, with 33 specimens (69% of the subsample),

are of unusually large types (locusts, all with $m > 1$ g and all but one, an outlier, with

perpendicular CLPPs). Because such large insects are not found in the migrant faunas at

the two localities (in England and Australia) where most ZLC-radar observations have

been made, some of the analyses reported here have been repeated with these specimens

excluded. The lepidopteran specimens comprise 28 species, many known to be

migratory; the mass range $100 < m \leq 300$ mg, with 54 specimens (57% of the

lepidopteran subsample), is perhaps disproportionately represented. Masses (for all

taxa) range from 9 mg to 4.1 g, the latter probably close to the upper limit for migrant

species; the range 550-1050 mg is unfortunately represented by only a single specimen.

Insert Table 1 near here

Selected results from C appeared in Riley (1985), but the values used here have

been recalculated from the original data and for α_2 and α_4 are mostly new, as are all the

S data. For A and W, the values used here are those recalculated by Hobbs and Aldhous

(2006), with α_2 reset negative for targets with $\theta_0 \approx 90°$ from the body axis (i.e. the

largest targets); further, because these authors used a different convention, the σ_{xx} and

σ_{yy} values for these large targets have been exchanged.

The values used in this analysis were obtained by the SM3 method of Hobbs and

Aldhous (2006), which ensures that α_2 and α_4 fall within (or on) the constraint

boundary of Equation (2). This in turn ensures that the RCS remains ≥ 0 at all

polarization angles, as required by definition. For C and S, SM3 estimates were

obtained with the *nlm* (Non-Linear Minimization) facility of the R data analysis system

(R Development Core Team 2008); the quantity minimized was the sum of squares of

the differences between the measured and fitted RCSs, over the full 360° range of

polarization angles ϕ. The fitted RCSs were calculated from the SM3 formula with fit

variables σ_{xx}, ε, β and θ_0 (Hobbs and Aldhous 2006, their equation 4; $\varepsilon^2 = \sigma_{yy}/\sigma_{xx}$ and β

is a phase). Values of the parameters a_0, α_2 and α_4 of Equation (1) were recovered as

$$a_0 = \sigma_{xx}(3 + 2\varepsilon \cos\beta + 3\varepsilon^2)/8 \qquad (4a)$$

$$\alpha_2 = \sigma_{xx}(1 - \varepsilon^2)/2\,a_0 \qquad (4b)$$

$$\alpha_4 = \sigma_{xx}(1 - 2\varepsilon \cos\beta + \varepsilon^2)/8\,a_0 \qquad (4c)$$

(Aldhous 1989, p. 21). Note that Equation (4b) automatically delivers the negative

values of α_2 discussed above for the targets for which $\sigma_{yy} > \sigma_{xx}$. Solutions were also

obtained via Equation (1) for verification purposes. They were mostly within 1% of the

SM3 values for a_0 and α_2 and often also for α_4, although there were some large

differences for this last parameter, usually when its value was <0.1. These 'harmonic'

solutions also helped to identify false minima in a small number of the SM3 fits, which

were then recalculated satisfactorily using different starting values. Some statistics for

the parameter values are provided in Table 2.

Insert Table 2 near here

In addition to these CLPP measurements, in order to extend the analysis of the

mass *vs* RCS relationship to low masses, limited use has been made of available values

of σ_{xx} and σ_{yy} for smaller insects, denoted L. Measurements (σ_{xx} only) of planthoppers

and aphids (both Hemiptera) made by JRR and G. A. Bent respectively were recovered

by digitising a graphic in Riley (1985). Measurements of ladybirds and other beetles,

lacewings (Neuroptera), moths, and hoverflies (Diptera) were made between 2000 and

2009 by JWC and ADS, working at Rothamsted Research; statistics or example values

for some of these have appeared previously (Chapman, Reynolds, et al. 2002; Chapman

et al. 2005, 2006). After exclusion of two large specimens that fall well within the range

for which CLPP measurements are available, L comprises 77 specimens of 15 species

and covers a mass range of 0.2−65 mg; there are mass values for all of these, but only

37 (48%) also have lengths and widths.

2.3.   *Measurements*

All CLPP measurements were made in laboratory rigs with the target at a distance of

~1 m from the antenna, which had a small aperture so that the target was in the far field.

For W a pulse-chirp radar system was used and only echo from the target's range was

recorded; the radar operated over frequencies ranging from 8 to 12 GHz and the results

are averages thought to represent a frequency of ~10 GHz. The other measurement

systems used continuous transmission at 9.4 GHz, the frequency used by almost all X-band entomological radars; they relied on absorptive materials, and for A a sky background, plus cancellation of non-target echo by passively returning an anti-phase signal via a directional coupler. Calibration was with metal spheres with RCSs extending over the range of RCSs being measured and placed at the target position; a calibration curve was fitted and its parameters used to convert measured echo intensities (recorded as a voltage) to RCSs. Measurements were made at ϕ intervals of 10° in C, 15° in W, and <1° in A and S. The S data subset includes repeated measurements of a small metal rod (length 16 mm, i.e. ~λ/2, and diameter ~1 mm) or 'dipole' that served to verify that the system performance had not altered. Further details for A, C, and W are available in the original publications (Aldhous 1989; Riley 1985; Wolf et al. 1993; Hobbs and Aldhous 2006); for S, the rig used was an upgraded version of that for C, with automated data acquisition at fine angular resolution.

The smaller insects in the L data subset were measured with a transmission-line (or 'rail-line') rig (Riley 1985). It was not practicable to measure the insect's angular position, and the σ_{xx} and σ_{yy} values were obtained by gluing the insect first vertically (σ_{yy} measurement) and then horizontally (σ_{xx} measurement) to a taut attachment line passing between the rails, with the insect oriented perpendicular to the rails (and parallel to the E-field) in the latter case.

Measurements were made with specimens that were either anaesthetized (A, W), freshly dead (some S, probably C), or freshly thawed after having been frozen (some S). As water is the main radio-reflective component of an insect it is important to measure both mass and the RCS properties before dehydration occurs; it appears that this was generally achieved. The legs of some of the large locusts in C drooped when the insect was mounted in the measuring rig, and for some of these the measurements were made

with the hind legs tied up with light thread to approximate the posture adopted by

locusts in 'cruising flight'. An investigation of a small sample indicated that specimens

with their legs drooping had CLPPs that were parallel, and thus very different from the

perpendicular patterns obtained from the same specimens with their legs tied up.

Measurements made with the legs down, or with one or both legs missing, have not

been used. Masses and body lengths were measured for all 156 specimens and abdomen

widths for all but one.

3.   Results

The RCS parameters for each specimen, along with specimen identifications, masses,

and dimensions, are provided in a supplementary spreadsheet file (Excel 2007,

Microsoft Corporation, Redmond, WA, USA; available via Figshare [Note to Editor:

please insert appropriate citation and link.]) containing two tables: the first with the

CLPP parameters (C, A, S, and W data) and the second with σ_{xx} and σ_{yy} values (L). The

following sections present analyses and interpretations of this ensemble of results.

3.1.   *Estimation of target mass*

With more measurements now available, it is appropriate to re-examine the relationship

of target mass to ZLC-observable size and shape parameters. As the parameter a_0 is a

measure of target size, it is the obvious quantity on which to base an estimate of mass

and a method depending on it alone is developed first. The possibility that improved

mass estimates can be obtained by additionally incorporating the shape parameters α_2

and α_4 is also explored.

3.1.1. *Polarization-averaged RCS and mass*

For a particular radar frequency and a particular target shape, the variation of the

target's RCS with its size passes through three regimes (Knott, Shaeffer, and Tuley 2004). In the 'Rayleigh region', where the target's longest dimension l is much smaller than the radio wavelength λ, the RCS σ increases with the sixth power of l, i.e. $\sigma \propto l^6$. At the opposite extreme, in the 'optical region', $\sigma \propto l^2$. Between these two is the transitional 'Mie region', in which the RCS passes through a small number of maxima and minima; these oscillations continue, with diminishing intensity, in the initial part of the optical region. This variation is well documented for water spheres (e.g. Drake & Reynolds 2012, pp. 51-54), for which the transition region is approximately $\lambda/5 \leq l \leq 5\lambda$. If this applies also to insects, then the two smallest specimens in the CLPP dataset ($l = 5$ mm, supplementary file) and about half of those in L just fall into the Rayleigh region and the remainder ($8 \leq l \leq 65$ mm) are Mie targets. The volume V of a target will vary as l^3 (again assuming a particular target shape). If migratory insects all have approximately the same density, so that their mass $m \propto V$, then $a_0 \propto m^2$ in the Rayleigh region; for (hypothetical) optical-region mega-insects, $a_0 \propto m^{2/3}$.

The variation of mass m with a_0 for the combined datasets is shown in Figure 1 using logarithmic scales for both variables. For the L data points, the σ_{xx} values were divided by a factor of 2.19, the average ratio of σ_{xx}/a_0 for the targets in the main dataset with $a_0 < 0.25$ cm^2 ($n = 18$, s. d. 0.24). It is apparent that there is a broad spread, with a range in $\log_{10}m$ of ~0.5 at most a_0 values. For a 1-cm^2 target, for example, this corresponds to a mass range of $60 \leq m \leq 180$ mg. This can be attributed to variations in shape and density between species, with a contribution also from experimental error. There is no evidence of maxima and minima, except perhaps in the extent of the spread which could originate from maxima and minima occurring at different a_0 values for insects with different morphological forms.

Insert Figure 1 near here

In order to estimate the masses of the targets detected by a ZLC radar, it is necessary to develop a mathematical relationship between m and a_0. From Figure 1, it is evident that a relatively simple, smooth, curve will suffice, and indeed is all that the data warrant. At low RCS values, the curve should exhibit the asymptotic Rayleigh m^2 dependence (i.e. $m \propto a_0^{1/2}$) and at high values it should approach $m \propto a_0^{3/2}$. It therefore can appropriately be represented by a spline, with two linear regions (on a log-log plot) joined by a curved form. For the latter, a simple polynomial may be sufficient. At the two transition points, the values of both functions and both first derivatives should be equal. (If they are not, discontinuities or obvious distortions will appear in distributions of mass values estimated from the relationship.) These requirements place constraints on the curve parameters, two of which, the slopes of the linear sections, are already known. The result is that if a second-order polynomial is employed to describe the link section, only two parameters plus the two transition points are free variables. Choice of transition points is not entirely free as they should conform approximately with the limits of the Rayleigh and optical regions.

Chapman, Smith, et al. (2002) have previously proposed an m vs a_0 relationship (Table 3), with parameters estimated from analyses of the C, A, and W data subsets, that conforms with these requirements to a good approximation. It uses a second-order curve in the Mie region, and while it does not employ an optical-region asymptote explicitly, the slope at the position of the largest target ($\log_{10}a_0 \approx 1.2$) is ~1.6, which is not much different from the asymptotic value of 1.5, so it is broadly consistent with this requirement. To determine the free Rayleigh-region parameter, they took account also of those elements of the L data subset that were then available. For the study dataset, the transition to the Rayleigh-region was fixed at $a_0 = 0.25$ cm^2, the value used by Chapman, Smith, et al. (2002), as this appears consistent with both theory and the data

(Figure 1), and the theoretical slope values for both asymptotic regions were adopted as

constants. The spline parameters were then obtained by treating the $\log_{10}a_0$ values as

independent variables and minimising the square of the residual between the $\log_{10}$-

transformed estimated and measured masses (Table 3, Figure 1). The constant,

quadratic, and (for the third-order case) cubic coefficients in the linking polynomial

were free and the remaining coefficients and the upper transition point determined from

their values. Minimization was carried out using the Solver function in Excel 2007,

using the default options; for the third-order case, it was necessary to identify the

appropriate solution of a quadratic equation for the upper transition point. The

minimizations converged without difficulty.

Insert Table 3 near here

The new relationship with a second-order linking section differs from that of

Chapman, Smith, et al. (2002) mainly by an offset in the estimated $\log_{10}m$ of from 0.11

to 0.17. The two curves run almost parallel to each other, crossing only at $a_0 \approx 15$ dBsc

($m \approx 20$ g), which is larger than any of the measured values (or any likely migrant

species). The effect is to increase the estimates of m by 25% for small insects and up to

39% for the largest species. The root-mean-square deviation for $\log_{10}m$ falls from 0.23

to 0.20, which is comparable with the range of variation apparent in Figure 1 (see

above) and corresponds to an uncertainty in mass of around ±50%. Introducing a third

order term to the polynomial reduces the r.m.s. deviation to 0.19; as the course of the

curve (not shown) changes only slightly and a slight sinuosity introduced in it appears

spurious, and as the upper transition point becomes unreasonably low, this more

complicated formula has not been adopted.

3.1.2. Mass estimation incorporating shape parameters

To explore whether the shape parameters α_2 and α_4 can contribute to the estimation of mass, we have undertaken a multiple-regression analysis with $\log_{10}m$ as the dependent variable and $\log_{10}a_0$, α_2 and α_4 as independent variables. This is of course possible only for targets for which the full CLPP was measured, i.e. for the C, A, S, and W data. No attempt has been made to merge the estimation relationship into the expected asymptotic forms in the Rayleigh and optical regions. However, the dataset includes some of the largest insects known to migrate and extends down to an a_0 value of 0.005 cm^2 (−23 dBsc, mass 9 mg; Table 2), which corresponds quite closely to the lower limit of target sizes that are detectable (Chapman, Smith, et al. 2002) or commonly detected (Drake 2013, 2016) with ZLC radars, so this is not a major defect.

A sequence of multiple linear regressions was undertaken, starting with a constant term plus a term linear in $\log_{10}a_0$ and then adding terms in $(\log_{10}a_0)^2$, α_2, and α_4. The quadratic term was included because the $\log_{10}m$ *vs* $\log_{10}a_0$ relationship must change slope over the a_0 range encompassed by the dataset (as discussed in the previous subsection where a quadratic relationship was also employed). Regressions were carried out using the *lm* (Linear Models) facility of R (R Development Core Team 2008) and assessed using analysis of variance (with R's *anova* facility). The results are summarized in Table 4. They show that a linear term in $\log_{10}a_0$ has the greatest explanatory power, and an α_2 term is more effective than a quadratic term in $\log_{10}a_0$ at further reducing the residual sum of squares and increasing the R^2. Adding either a quadratic term in $\log_{10}a_0$ or an α_4 term to the combination of $\log_{10}a_0$ (linear) and α_2 provides no significant further improvement. A scatterplot of α_2 *vs* a_0 (not shown) reveals that $\alpha_2 > 0.5$ for $a_0 < 0$ dBsc but it decreases steadily above this point and is negative for $a_0 > 3$ dBsc, so the value of this parameter provides information on the

higher masses that occur above the Rayleigh region (i.e. the upturn in slope in Figure 1

at $a_0 \approx 0$ dBsc). A linear term in α_2 apparently does this more effectively than a

quadratic term in $\log_{10}a_0$, with the former giving an uncertainty on the mass estimates of

±40% (residual standard error on $\log_{10}m$ of 0.16) and the latter ±60% (0.24). The α_4 *vs*

a_0 plot (also not shown) exhibits a less clear and more scattered dependence of α_4 on a_0,

so it is unsurprising that this parameter makes almost no additional contribution.

Insert Table 4 near here

Aldhous (1989), using only the A data subset, explored how mass varied with

several RCS quantities and found approximately linear relationships for $\log_{10}m$ *vs*

$\log_{10}\sigma_{le}$, where σ_{le} is the lesser of σ_{xx} and σ_{yy}, and for $\log_{10}m$ *vs* $\log_{10}(\sigma_{xx}/\sigma_{yy})$. (These

σ_{xx} and σ_{yy} are as defined here rather than in the original publication; see section 2.2.)

Scatterplots (not shown) demonstrate that these relationships retain their quasi-linear

form with the full CLPP dataset. We have therefore explored including these terms in

the regression as an alternative to α_2 (Table 4). It was found that $\log_{10}\sigma_{le}$ provides only

modest additional explanatory power but $\log_{10}(\sigma_{xx}/\sigma_{yy})$ performs almost as well as α_2.

3.2.   Shape as an identification character

3.2.1. Radar shape and taxonomic group

The distribution of the shape parameter pairs (α_2, α_4) over the allowed region of the

(α_2, α_4) plane is shown for the full CLPP dataset in Figure 2(a). It can be seen that

$\alpha_4 < 0.5$ for all but one specimen and that pairs are found across much of the right-hand

half ($\alpha_2 > 0$) of the $\alpha_4 < 0.5$ part of the allowed area but are confined to a more

restricted region ($\alpha_4 < 0.3$) of the left-hand half. There is a concentration of targets on or

close to the boundary where $\alpha_2 \approx 1.0$, a region corresponding approximately to the

'main cluster' identified in analyses of ZLC-radar observations of target shape (Dean

and Drake 2005, Drake 2016). There are relatively few targets in the region $0 < \alpha_2 \leq 0.5$ and only one of these has $\alpha_4 < 0.2$; the equivalent region of the left-hand half, however, is crowded.

Insert Figure 2 near here

Lepidopteran specimens extend throughout the right-hand half of the figure but are most numerous in or close to the main-cluster region; there is only one specimen with $\alpha_2 < 0$. Orthopterans occur in both halves but only two fall into the main cluster; orthopterans in the right-hand half mostly have $\alpha_4 > 0.2$. The specimens from other orders all fall into the right-hand half, some in the main cluster but others well away from the boundary; this is a morphologically mixed group so a variety of (α_2, α_4) combinations is to be expected. The figure also shows the results for the dipole; they fall along the boundary where α_2 is approaching its maximum possible value and, reassuringly, show little spread.

In order to explore these patterns more precisely, a main-cluster region (MCR) will be defined in terms of the orthogonal variables (p, q) as these delineate it very nicely (Figure 2(b)). There are 79 specimens in the MCR, of which 2 are Orthoptera, 68 are Lepidoptera, and 9 are other taxa; of the 77 specimens falling outside the MCR, 46 are Orthoptera, 26 Lepidoptera, and 5 other. The uneven distribution of orthopterans and lepidopterans is significant (G-test for a model-I 2×2 contingency table with Yates correction, $G = 69.3$, 1 d.f., $P < 0.001$; Sokal and Rolf 1995, ch. 17); it remains significant, though at a lower level, if the specimens with perpendicular CLPPs (32 locusts, 1 moth) are excluded ($G = 21.8$, $P < 0.001$).

3.2.2. *Relation of radar shape to mass and morphology*

The location of a specimen on the (α_2, α_4) plane will be determined by its size and

general morphology, with these represented by the parameters m, l, w, and f. A

relatively clear pattern emerges when the symbols for the points on the (α_2, α_4) plane

indicate the specimen's mass (Figure 2(b)). All specimens in the left-hand half of the

allowed region have $m > 600$ mg and only one specimen (an outlier – see below) in the

right-hand half exceeds this mass. All but two of the lightest specimens ($m \leq 100$ mg,

$n = 29$) occur in the MCR, as do 49 (73%) of the intermediate-mass insects

($100 < m \leq 300$ mg, $n = 67$). The remaining population of the MCR comprises 3 insects

with $300 < m \leq 400$ mg, which constitutes 5% of the heaviest specimens ($m > 300$ mg,

$n = 60$). The mass difference between specimens in the MCR and those falling outside it

is significant (Wilcoxon rank sum test, two-sided, $n_1 = 79$, $n_2 = 77$, $W = 333$, P

< 0.001). Inspection of Figure 2(b) suggests that in the MCR and further inwards, in the

adjoining 'MCR Extension' (MCRE; Figure 2(b)), there is a general increase of target

mass with distance from the boundary. Further, for specimens outside the MCR, there

appears to be a trend of mass increasing from top-right ($\alpha_2 \approx 1.4$, $\alpha_4 \approx 0.5$) to bottom-

mid-left ($\alpha_2 \approx -0.7$, $\alpha_4 \approx 0.05$). The latter phenomenon is the same as that noted in

section 3.1 where α_2 (if signed as here) was found to be a useful predictor of mass. As is

to be expected from the analysis of section 3.1, there is also a significant difference in

a_0 values between the specimens in the MCR and outside it ($W = 705$, $P < 0.001$). The

pattern of a_0 values across the (α_2, α_4) plane (not shown) is similar to that for mass,

though the variance appears greater and this makes the trends somewhat less evident.

Regression analyses (Table 5) show that the trends are significant. However, the

decrease of mass with increasing p within the combined MCR and MCRE regions has a

modest adjusted r^2 and accounts for only 29% of the sum of squares. Four points with

very low mass ($9 \leq m \leq 14$ mg) appear as outliers, but this is essentially an artefact of

the measurement sample in which low masses are under-represented: it appears likely

that inclusion of more insects with $m < 40$ mg would further reduce the r^2 and the sum

of squares accounted for. Adding a q term into the regression produces negligible

improvement. For the non-MCR specimens, the adjusted r^2 indicates a strong

dependence of mass on α_2, with this parameter accounting for 86% of the sum of

squares; two outlier points here are due to specimens that arguably belong in the MCR

as they have masses (49, 82 mg) lower than the rest (≥ 173 mg) and q values that only

just fall outside the nominal MCR limits. An added α_4 term is marginally significant but

accounts for only a further 1% of the sum of squares. When $\log_{10}a_0$ rather than $\log_{10}m$ is

made the dependent variable, the results (Table 5) are similar, though the adjusted r^2

values are lower and smaller proportions of the sum of squares are accounted for. These

weaker statistics reflect the less strong trends and greater variance discerned through

inspection of the plots (previous paragraph). The trend statistics for the non-MCR

specimens are obviously strengthened by the large number of $m > 1$ g specimens (all

locusts) with their extreme values of both α_2 and the response variables m and a_0.

Excluding these leaves a still significant relationship for $\log_{10}m$ but not for $\log_{10}a_0$

(Table 5). If the two low-mass specimens that arguably belong in the MCR are also

excluded, the adjusted r^2 for $\log_{10}m$ rises to 0.77 (though that for $\log_{10}a_0$ is not

improved). Similar weak trends for $\log_{10}a_0$ in these two regions were noted in an

analysis of a single night of ZLC-radar observations at an Australian site (Dean and

Drake 2005).

Insert Table 5 near here

Differences between the MCR and non-MCR specimens are also evident when

the specimen character indicated is the length, width, or form (Figure 3; detailed results

not presented), and these are statistically significant (Wilcoxon test, $n_2 = 77$ for l but 76

for w and f, $P < 0.001$). Regressions of l, w, and f against p for the specimens in the

combined MCR and MCRE account respectively for 16, 5, and 1% of the sum of squares, with the p coefficient significant at the $P < 0.001$ level for l, at < 0.05 for w, and not significant (~ 0.3) for f. For the non-MCR specimens regressed against α_2, the proportions are 81, 10, and 37% respectively with P values < 0.001, 0.007, and < 0.001; with the $m > 1$ g locusts excluded, the proportions are 36, 30, and 9% with P values < 0.001, < 0.001, and 0.05. Thus the length shows differences and trends similar to those for m and a_0, but for the width and form the trends are less clear.

Insert Figure 3 near here

Two additional regression analyses have been undertaken for the form f to examine its potential for providing information orthogonal to that from a_0. For the CLPP data, adding q into the regression of f against p in the combined MCR and MCRE increases the sum of squares accounted for, but only to 2% and neither parameter is significant. Adding α_4 into the regression of f against α_2 for all non-MCR specimens provides negligible improvement; however, with the locusts excluded the proportion accounted for increases to 20% and this is also achieved with α_4 alone.

For the small specimens in the L subsample, the available radar measure of shape is the ratio r_{sh} (i.e. σ_{xx}/σ_{yy}). The form f shows a significant relationship with r_{sh} for these specimens (Figure 4(a); $n = 39$, coefficient 0.224 ± 0.028, intercept 1.28 ± 0.34, 64% of variance accounted for, $P < 0.001$). Two clusters apparent in this plot are due to single-species groups, but other species show a broad spread of r_{sh} values (Figure 4(a)). A similar analysis for the mostly larger CLPP specimens, with r_{sh} calculated from α_2 and α_4 via Equations 3 (and after excluding two specimens with $r_{sh} > 50$), shows no relationship (Figure 4(b); $n = 121$, $P \approx 0.8$). This is still the case if only specimens with $m \leq 80$ mg, i.e. in the same mass range as those in the L subsample, are included ($n = 15$, $P \approx 0.6$), and also if the range is extended slightly to $m \leq 100$ mg in order to

enlarge the sample ($n = 27$, $P \approx 0.6$). Thus for targets with $a_0 \leq 0.25$ cm^2 (which from

Table 3 corresponds to $m \leq 80$ mg), f can be estimated as

$$f = 0.224 r_{sh} + 1.28 . \qquad (5)$$

Because of the uncertainties on these parameters, the 1-standard deviation uncertainty

on f will increase from ±0.3 to ±0.9 over the range $0 < r_{sh} \leq 20$. The data provide no

basis for estimating f for targets with $a_0 > 0.25$ cm^2.

Insert Figure 4 near here

3.2.3. Mass and morphology associated with different radar shapes

An alternative way of representing these relationships is to determine where insects of

different sizes or shapes are located in the (α_2, α_4) plane. In the case of mass (Figure 5),

insects with $m \leq 150$ mg are found entirely in the MCR; those with $150 < m \leq 250$ mg

occupy both the MCR and the MCRE and are also found in the adjacent area to the right

($q > 1.5$) of these; those with $250 < m \leq 400$ mg are predominantly in the MCRE; those

with $400 < m \leq 1000$ mg are in the area adjacent and to the left of the MCRE (with

$0 < q \leq 0.8$), and almost all of those with $m > 1$ g fall into the left-hand half of the

diagram (where q is considered negative), with the largest ($m > 2$ g) slightly further to

the left. All but three of the 13 lightest insects ($m \leq 70$ mg) occur along the outer

periphery of the MCR, with $p > 0.95$. A trajectory traced through the plane by a

notional 'typical insect' as its mass increases can thus be identified, though it is broad in

extent (Figure 6). (It should be noted that variance in mass occurs along the trajectory,

on the scale indicated by the distance across the ellipses, as well as laterally.) The mass

ranges associated with the regions of Figure 6, and the number of specimens falling

within or near them, are presented in Table 6. Region C, which contains only a small

number of specimens, is tentatively identified as a spur off the main trajectory.

Insert Figure 5 near here

Insert Figure 6 near here

Similar trends are evident for RCS a_0 and length l (Table 6), although these

characters partition the specimens into the regions less precisely than does m. As

specimens with similar widths w occur in both the left- and right-hand sides of the plane

(not shown), there is no equivalent trend for this character. For the form f, specimens

with $f \leq 6$ ($n = 102$) fall within regions A, B, D and E while those with $f > 6$ fall

predominantly ($n = 31$) into the left-hand half of the plane with the remainder ($n = 22$)

scattered widely across the right hand half. The specimens in region C and close to the

constraint boundary ($n = 5$) had narrow bodies ($2 < w \leq 3$ mm) and lengths in the range

$20 < l < 22$ mm (giving $6 < f < 8$; all were *Chorthippus brunneus*, a grasshopper. Their

location was the closest to that of the metal dipoles (Figure 2), which are also very

narrow (~1 mm) and made to a length, 16 mm, that will produce resonance when

aligned with the E field. The RCS values of the five *C. brunneus* specimens were ~1 dB

higher than predicted (from relationship of Table 5) for their ~200 mg mass, so it is

possible that they were at or near resonance too. Two smaller specimens of this species,

with $l \approx 16$ mm and $f \approx 8$, fell into region B. Several of the small L specimens have

$r_{sh} \geq 10$ (and $f \geq 2.6$, Figure 4), and from this it can be inferred that they lie in the right-

hand parts of the A, B, or C regions (Figure 6, which shows contours of f). The ladybird

beetles, with $f \approx 1.3$, have $r_{sh} \leq 4.3$ and therefore must fall to the left of A and B; their

α_4 values are unknown but given their low masses ($11 \leq m \leq 32$ mg), it seems likely

(see Figure 5) that they lie close to the constraint boundary.

Insert Table 6 near here

3.2.4. Identification of perpendicular CLPPs

As noted above, when targets are observed with a ZLC-radar (as opposed to in a

laboratory rig), there is a possibility of a 90° error in the retrieved alignment. The

question of whether this can be resolved from the radar observations themselves is

examined here by direct reference to the dataset. In this sample, and after eliminating

one outlier point, the transition to perpendicular CLPPs occurs around $m \approx 600$ mg

(Figure 2b) and in the zone $3 < a_0 \leq 4$ dBsc. Unfortunately the dataset includes only one

specimen in the $500 < m < 1000$ mg transition region, so the transition behaviour cannot

be discerned in any detail.

4.   Discussion

The measure of size provided by a ZLC radar is the polarization-averaged RCS a_0 and

an established monotonic relationship between this and mass has been verified, and its

parameters refined, in this work. Masses estimated from a_0 have an uncertainty of

$\sim \pm 60\%$, but given the wide range of insect sizes this still provides useful discrimination.

If the shape parameter α_2 is incorporated into the mass-estimation procedure the

uncertainty can be reduced to $\sim \pm 40\%$, but seamless linking into the lower and upper

asymptotic regions will then be lost so this is feasible only when small or very large

insects are absent or of no interest. Use of a spline quadratic in $\log_{10} a_0$ to link

appropriate linear asymptotic slopes (Table 3, line 2) appears adequate and robust and

leaves the shape parameters as independent identification variables; this relationship is

therefore recommended for general use.

An important finding from this research is that the values of α_2 and α_4, the

primary shape parameters, are determined mainly by the size of the insect, as

represented either by its mass or its length. Small and medium-sized insects, with

$m \leq 150$ mg and $l \leq \sim 20$ mm, are almost completely confined to regions A and B of the

(α_2, α_4) plane (Figure 6), an area also known as the MCR and identified previously

from ZLC observations of nocturnal insect migration. As insect size increases beyond

150 mg the CLPP parameters follow a broad trajectory, moving initially away from the

constraint boundary (i.e. α_4 increasing) into region D and then leftwards (α_2

decreasing) into E, passing into the left-hand half of the plane (α_2 negative, CLPP

perpendicular) at a mass of around 600 mg (region F) and getting close to the lower left-

hand boundary (α_2 and α_4 both decreasing, region E) at ~ 4 g. Narrow ($w \leq 3$ mm)

insects with $m \approx 200$ mg and $l \approx 20$ mm may be found off this main trajectory in region

C.

These major variations of α_2 and α_4 with m, and hence also with a_0, mean that

these parameters do not form a naturally orthogonal system with a_0. The trajectory is

broad, and the obvious candidate for orthogonality is the transverse direction. This

changes as m increases, meaning that different relationships would have to be sought in

different regions. Symmetry considerations require that a perfectly round insect will

have a circular CLPP, i.e. one with $\alpha_2 = \alpha_4 = 0$, and basic consideration of

electromagnetic scattering leads to the expectation that the CLPPs of elongated insects

are unlikely to be circular, and that the patterns for insects of the same mass but

differing degrees of elongation (i.e. different forms) will not be the same, so some

degree of orthogonality seems assured. The obvious relation to test, therefore, is one

between form and a quantity representing the transverse direction; the latter could be α_2

or q in regions A, B and D and α_4 in regions C-G. Regression analyses found no

contribution from q in the former region and only a moderate one from α_4 in the latter.

In contrast to these results which suggest there is little prospect of estimating f

from the radar data for the larger insects ($m > \sim 80$ mg) predominating the CLPP sample,

Chapman, Reynolds, et al. (2002) and Chapman et al. (2005, 2006) were able to use

shape to discriminate between targets when observing very small ($m \leq 13$ mg) species.

They used the ratio $r_{sh} = \sigma_{xx}/\sigma_{yy}$ as their identification parameter, with values

determined by laboratory measurements (and included here in L) of around 10, 10, and

20 for diamondback moths, carabid beetles, and lacewings respectively. In this study, a

linear relationship between r_{sh} and f was found for the full L sample ($m \leq 81$ mg), but

not for a smaller sample of the specimens of similar size in the CLPP sample. That a

relationship between radar shape and morphological form should be more apparent for

small insects (targets falling into the Rayleigh region, or close to it) than for larger ones

(Mie region) is not altogether unexpected given the more complicated radio-wave

scattering processes involved with the latter which lead, at higher masses, to the

transition to perpendicular CLPPs. Given that r_{sh} broadly increases with α_2 (Figure 6),

there is no reason to expect it to have any advantage as a discriminating variable for

specimens larger than those in L.

The majority of targets detected so far with ZLC-radars have $a_0 < 3$ dBsc (e.g.

Drake 2016), which the results presented here indicate is in the range where CLPPs are

parallel rather than perpendicular. Thus target alignments can confidently be attributed

to the direction of the maximum axis of the CLPP. An attempt to detect this transition in

a single night's observations at an Australian site was unsuccessful, even though the

radar seemed to indicate that a small number of sufficiently large targets were present

(Dean and Drake 2005). Operation of a unit in a region where large locusts, or other

species of similar size, are known to be present in the aerial fauna may be necessary to

verify that orientations of such targets are at right angles to the observed CLPP axis, and

to better determine the a_0 value at which the transition occurs.

The measurement sample analyzed in this work includes many migrant species, but it is not representative of the migrant fauna at any particular location. However, a study of radar characters of insects detected at the Australian site over an eight-month period identified peaks in the A, B, D and E regions of the (α_2, α_4) plane, but not in C or the region to the left of A and B (Drake 2016). Moreover, the peaks found by that study in regions A and B (the MCR) were almost all centred at $a_0 \leq \sim-5$ dBsc, with some extending up to 0 dBsc (masses of ~90 and ~200 mg respectively, Figure 1), which agrees reasonably with the $m \leq 150$ mg range determined here (Table 6). Peaks in the D and E regions in the Australian study almost all had $0 < a_0 \leq 5$ dBsc (i.e. $200 < m < 850$ mg), which again is consistent with this work. The Australian data suggest that the possibly resonant behaviour of the *C. brunneus* specimens in the measurement dataset may be relatively unusual. They also indicate that the measurement sample, with the large locusts ($m > 1$ g) excluded, is reasonably representative of the Australian migrant fauna (even though the great majority of the species measured do not occur in Australia). Perhaps migrant insect faunas do not differ morphologically very much from one continent to another: while the species differ, at higher taxonomic levels there is much commonality (e.g. Johnson 1969) and as the phenomena of nocturnal migration are broadly similar from region to region (e.g. Drake & Gatehouse 1996, Drake & Reynolds 2012) it can be expected that the adaptations leading to them will be too. The results from this study should therefore have wide applicability.

Acknowledgments

References

Aldhous, A. C. 1989. "An Investigation of the Polarization Dependence of Insect Radar

Cross Sections at Constant Aspect." PhD thesis, Cranfield Institute of

Technology. Available at https://dspace.lib.cranfield.ac.uk/handle/1826/2041

Chapman, J. W., A. D. Smith, I. P. Woiwod, D. R. Reynolds, and J. R. Riley. 2002.

"Development of Vertical-looking Radar Technology for Monitoring Insect

Migration." *Computers and Electronics in Agriculture* 35:95–110.

doi:10.1016/S0168-1699(02)00013-3

Chapman, J. W., D. R. Reynolds, A. D. Smith, J. R. Riley, D. E. Pedgley, and I. P.

Woiwod. 2002. "High-altitude Migration of the Diamondback Moth *Plutella

xylostella* to the U.K.: a Study Using Radar, Aerial Netting and Ground

Trapping." *Ecological Entomology* 27:641-650. doi:10.1046/j.1365-

2311.2002.00472.x

Chapman, J. W., D. R. Reynolds, A. D. Smith, J. R. Riley, M. J. Telfer, and I. P.

Woiwod. 2005. "Mass aerial migration in the carabid beetle *Notiophilus

biguttatus*." *Ecological Entomology* 30:264-272. doi:10.1111/j.0307-

6946.2005.00702.x

Chapman, J. W., D. R. Reynolds, S. J. Brooks, A. D. Smith, and I. P. Woiwod. 2006.

"Seasonal Variation in the Migration Strategies of the Green Lacewing

Chrysoperla carnea Species Complex." *Ecological Entomology* 31: 378-388.

doi: 10.1111/j.1365-2311.2006.00797.x

Chapman, J. W., R. L. Nesbit, L. E. Burgin, D. R. Reynolds, A. D. Smith, D. R.

Middleton, and J. K. Hill. 2010. "Flight Orientation Behaviors Promote Optimal

Migration Trajectories in High-Flying Insects." *Science* 327: 682-685.

doi:10.1126/science.1182990

Dean, T. J. 2007. "Development and Evaluation of Automated Radar Systems for

Monitoring and Characterising Echoes from Insect Targets." PhD thesis, The

University of New South Wales. Available at

http://handle.unsw.edu.au/1959.4/38667

Dean, T. J., and V. A. Drake. 2005. "Monitoring Insect Migration with Radar: The

Ventral-aspect Polarization Pattern and its Potential for Target Identification."

International Journal of Remote Sensing 26:3957–3974. doi:

10.1080/01431160500165955. doi:10.1080/01431160500165955.

Dingle, H. 2014. *Migration. The Biology of Life on the Move*. 2nd ed. Oxford: Oxford

University Press.

Drake, V. A. 2002. "Automatically Operating Radars for Monitoring Insect Pest

Migrations." *Entomologia Sinica* 9 (4):27–39. doi:10.1111/j.1744-

7917.2002.tb00169.x

Drake, V. A. 2016. "Distinguishing target classes in observations from vertically

pointing entomological radars." *International Journal of Remote Sensing* 37**,**

3811-3835. doi: 10.1080/01431161.2016.1204028

Drake, V.A. and A. G. Gatehouse (eds). 1995 *Insect Migration: Tracking Resources

through Space and Time*. Cambridge, UK: Cambridge University Press.

Drake, V. A., and D. R. Reynolds. 2012. *Radar Entomology. Observing Insect Flight

and Migration.* Wallingford, UK: CABI.

Drake, V. A., and H. K. Wang. 2013. "Recognition and Characterization of Migratory

Movements of Australian Plague Locusts, *Chortoicetes terminifera*, with an

Insect Monitoring Radar." *Journal of Applied Remote Sensing* 7:075095, 17 pp.

doi: 10.1117/1.JRS.7.075095.

Dudley, R. 2000. *The Biomechanics of Insect Flight: Form, Function, Evolution.*

Princeton: Princeton University Press.

Frick, W. F., P. B. Chilson, N. W. Fuller, E. S. Bridge, and T. H. Kunz. 2013.

"Aeroecology." In *Bat Evolution, Ecology, and Conservation*, edited by R. A.

Adams and S. C. Pedersen, 149–167. New York: Springer.

Hobbs, S. E., and A. C. Aldhous. 2006. "Insect Ventral Radar Cross-section Polarisation

Dependence Measurements for Radar Entomology." *IEE Proceedings – Radar,*

Sonar and Navigation 153: 502-508. doi:10.1049/ip-rsn:20060019

Hu, G., K. S. Lim, N. Horvitz, S. J. Clark, D. R. Reynolds, N. Sapir, and J. W.

Chapman. 2016a. "Mass Seasonal Bioflows of High-flying Seasonal Migrants."

Science 354: 1584-1587.

Hu, G., K. S. Lim, D. R. Reynolds, A. M. Reynolds, and J. W. Chapman. 2016b.

"Wind-Related Orientation Patterns in Diurnal, Crepuscular and Nocturnal

High-Altitude Insect Migrants." *Frontiers in Behavioral Neuroscience* 10 article

32 (8 pp.). doi:10.3389/fnbeh.2016.00032

Isard, S. I., and S. H. Gage. 2001. *Flow of Life in the Atmosphere: an Airscape*

Approach to Understanding Invasive Organisms. East Lansing: Michigan State

University Press.

Johnson, C. G. 1969. *Migration and Dispersal of Insects by Flight*. London: Methuen.

Knott, E. F., J. F Shaeffer, and M. T. Tuley. 2004. *Radar Cross Section*. 2nd ed.

Rayleigh, NC: SciTech Publications.

Koul, O., G. W. Cuperus, and N. Elliot. (eds). 2008. *Areawide Pest Management:*

Theory and Implementation. Wallingford, UK: CAB International.

Melnikov, V. M., M. J. Istok, and J. K. Westbrook. 2015. "Asymmetric Radar Echo

   Patterns from Insects." *Journal of Atmospheric and Oceanic Technology* 32:

   659-674. doi: 10.1175/JTECH-D-13-00247.1.

Mirkovic, D., P. M. Stepanian, J. F. Kelly, and P. B. Chilson. 2016. "Electromagnetic

   Model Reliably Predicts Radar Scattering Characteristics of Airborne

   Organisms." *Scientific Reports* 6, article 35637. doi:10.1038/srep35637

R Development Core Team. 2008. *R: A language and environment for statistical

   computing*. Vienna, Austria: R Foundation for Statistical Computing.

   http://www.R-project.org.

Reynolds, A. M., D. R. Reynolds, S. P. Sane, G. Hu, and J. W. Chapman. 2010.

   "Orientation in High-flying Migrant Insects in Relation to Flows: Mechanisms

   and Strategies." *Philosophical Transactions of the Royal Society B* 371:

   20150392283. doi:10.1098/rstb.2015.0392

Riley, J. R. 1985. "Radar Cross Section of Insects." *Proceedings of the IEEE* 73: 228-

   232. doi:10.1109/PROC.1985.13135

Sokal, R. R., and F. J. Rohlf. 1995. *Biometry: the Principles and Practice of Statistics

   in Biological Research*. 3rd ed. New York: W. H. Freeman.

Wang, H.K. 2008. "Evaluation of Insect Monitoring Radar Technology for Monitoring

   Locust Migrations in Inland Eastern Australia." PhD thesis, The University of

   New South Wales. Available at http://handle.unsw.edu.au/1959.4/38923

Wolf, W. W., C. R. Vaughn, R. Harris and G. M. Loper. 1993. "Insect Radar Cross-

   sections for Aerial Density Measurements and Target Classification."

   Transactions of the American Society of Agricultural Engineers 36: 949-954.

   doi:10.13031/2013.28420

Table 1. Composition and sources of the CLPP dataset[a].

Taxonomic group	Source				
	C	A	W	S	All
Orthoptera	5, 30	2, 18	0, 0	0, 0	6, 48
Lepidoptera	1, 13	15, 34	3, 5	13, 42	28, 94
others[b]	1, 1	1, 2	3, 9	1, 2	6, 14
All	7, 44	18, 54	6, 14	14, 44	40, 156

[a]Number of species, number of specimens. See text (section 2.2) for details of sources C, A, W and S.

[b]Bees and wasps (Hymenoptera) (2, 7), beetles (Coleoptera) (2, 3), craneflies (Diptera) (2, 4).

Table 2. Summary of masses and RCS parameter values for the CLPP dataset.

Taxonomic group	Mass	RCS parameter		
	m (mg)	a_0 (dBsc)	α_2	α_4
Orthoptera	1597 (68, 4120)	4.6 (0.39, 16.8)	−0.03 (−0.90, 1.31)	0.20 (0.01, 0.56)
Lepidoptera	194 (9, 648)	0.98 (0.013, 2.72)	0.91 (−0.10, 1.22)	0.23 (0.08, 0.43)
others[b]	114 (10, 220)	0.51 (0.005, 1.48)	0.94 (0.62, 1.27)	0.22 (0.09, 0.48)
All taxa	618 (9, 4120)	2.04 (0.005, 16.8)	0.62 (−0.90, 1.31)	0.22 (0.01, 0.56)

[a]Average (minimum, maximum).

[b]As in Table 1.

Table 3. Parameters of mass *vs* RCS relationships[a]

Origin	Region			
$(\log_{10}m$ r.m.s.$)$	Lower[b]	Linking	Upper	Upper transition[c]
Chapman et al. (2002) (0.23)	2.097 0.5	2.205 0.8729 0.3323	–	–
This study, second order. (0.20)	2.207 0.5 (81 mg)	2.331 0.9124 0.3425	2.079 1.5	0.8580 (7.21 cm^2 2.32 g)
This study, third order. (0.19)	2.243 0.5 (88 mg)	2.249 0.8028 0.9583 0.7826	2.1459 1.5	0.2605 (1.87 cm^2, 359 mg)

[a]Parameters are for the relationship of $\log_{10}m$ to $\log_{10}a_0$. (Note a_0 (dBsc) is $10\log_{10}a_0$.) The first value in each list is the constant term, the second the coefficient of $\log_{10}a_0$, and so on for higher powers of $\log_{10}a_0$ if these are present.

[b]Transition from the lower to the linking curve was fixed at $\log_{10}a_0 = -0.60206$ (i.e. $a_0 = 0.25$ cm^2) for all curves. Value in parenthesis is the corresponding mass m.

[c]First value is $\log_{10}a_0$; values in parenthesis are a_0 and the corresponding mass m.

Table 4. Results of multiple linear regression analyses of m vs (a_0, α_2, α_4) relationships

Model[a] (note)	Coefficients	ANOVA sum of squares, (P), [residual].	Adjusted R^2, residual standard error.	Degrees of freedom, F, (P).
Constant $\log_{10}a_0$	2.418 0.829	– 35.93 (<0.001) [11.29]	0.759 0.271	1, 154 490 (<0.001)
Constant $\log_{10}a_0$ $(\log_{10}a_0)^2$	2.345 0.9378 0.2156	– 35.93 (<0.001) 2.578 (<0.001) [8.709]	0.813 0.239	2, 153 338 (<0.001)
Constant $\log_{10}a_0$ α_2 (See note b)	2.712 0.5068 −0.4655	– 35.93 (<0.001) 7.334 (<0.001) [3.953]	0.915 0.161	2, 153 837 (<0.001)
Constant $\log_{10}a_0$ $\log_{10}\sigma_{le}$	2.645 0.2591 0.4343	– 35.93 (<0.001) 2.831 (<0.001) [8.457]	0.819 0.235	2, 153 351 (<0.001)
Constant $\log_{10}a_0$ $\log_{10}(\sigma_{xx}/\sigma_{yy})$	2.705 0.5106 −0.4315	– 35.93 (<0.001) 7.009 (<0.001) [4.278]	0.908 0.167	2, 153 768 (<0.001)

[a]Dependent variable is $\log_{10}m$.

[b]Adding $(\log_{10}a_0)^2$ reduces sum of squares by 0.07 (0.2%), coefficient not significant (P ~0.09). Adding α_4 reduces sum of squares by 0.04 (0.1%), coefficient not significant (P ~0.2).

Table 5. Results of regression analyses of m and a_0 vs (p, q) and (α_2, α_4).

Region and dependent variable[a]	Model [2nd model][b]	Coefficients	Sum of squares, (P)[c], [residual].	Adjusted r^2, residual standard error.	Degrees of freedom, F, (P).
MCR and MCRE $\log_{10}m$	Constant p [q, 0.9, 0.02%]	3.35 −1.39	– 2.88 (<0.001) [6.95]	0.29 0.27	1, 98 41 (<0.001)
MCR and MCRE $\log_{10}a_0$	Constant p [q, 0.2, 1%]	1.07 −1.50	– 3.36 (<0.001) [21.34]	0.13 0.47	1, 98 15 (<0.001)
All except MCR $\log_{10}m$	Constant α_2 [α_4, 0.02, 1%]	2.97 −0.66	– 14.57 (<0.001) [2.39]	0.86 0.18	1, 75 456 (<0.001)
All except MCR $\log_{10}a_0$	Constant α_2 [α_4, 0.2, 0.9%]	0.47 −0.46	– 7.02 (<0.001) [4.41]	0.61 0.24	1, 75 120 (<0.001)
All except MCR ($m > 1$ g excluded) $\log_{10}m$	Constant α_2 [α_4, 0.003, 9%]	2.74 −0.41	– 0.99 (<0.001) [0.89]	0.52 0.15	1, 42 47 (<0.001)
All except MCR ($m > 1$ g excluded) $\log_{10}a_0$	Constant α_2 [α_4, 0.6, 0.6%]	0.22 −0.18	– 0.19 (0.07) [2.22]	0.06 0.23	1, 42 3.6 (0.07)

[a]MCR, MCRE – Main Cluster Region, MCR Extension (see sections 3.2.1, 3.2.2).

[b]The second model incorporates an additional independent variable; this variable, its P value, and the additional reduction in the sum of squares it produces (expressed as a proportion), are provided.

[c]From ANOVA; sum of squares accounted for by the variable, and P value for that variable.

Table 6. Predominant regions of the (α_2, α_4) plane for different insect characters

Mass m (mg)			RCS a_0 (dBsc)			Length l (mm)		
Range	Number[a]	Region[b]	Range	Number	Region	Range	Number	Region
<70	13	A				<12	6	A
70-150	46	A, B	<–2[c]	45	A, B			
150-250[x]	32	B, C	–2-0	25	B, D	12-22	87	A, B, C
250-400	22	D	0-4[d]	50	B, C, D, E	22-25	17	D
400-1000	10	E				25-30	12	E
1000-2000	15	F	>4	35	F, G	>30	33	F, G
>2000	17	G						

[a]Total 155 as specimen with no width measurement excluded from analysis.

[b]See Figure 6, but note that the ellipses there are schematic and indicate a general area.

Figure captions

Figure 1. Relation of measured insect masses m (mg) to polarization-averaged RCSs a_0 (dBsc) for the study dataset. Key: • – CLPP averages; + – estimated from σ_{xx}; × – water-filled capillary tube, estimated from σ_{xx}; main curve – fitted spline (Table 3), with linear sections dashed and the second-order section continuous; short-dashed lines – Chapman, Smith, et al. (2002) fit, of which for clarity only the ends are shown.

Figure 2. (a) Positions of the CLPP dataset specimens on the (α_2, α_4) plane; $n = 156$. The solid line indicates the constraint boundary (Equation (2)). The area within the dashed rectangle is shown enlarged at right. Key: ○ Orthoptera ($n = 48$), + Lepidoptera ($n = 94$), △ other orders ($n = 14$), □ dipole ($n = 7$). (b) As (a) but with the dipoles omitted and symbols representing the specimen's mass (see key on plot) and the MCR (Main Cluster Region, $0.8 < p \leq 1$, $0.7 < q \leq 1.5$) and MCRE (MCR Extension, $0.5 < p \leq 0.8$, same q range) indicated.

Figure 3. As Figure 2b but with size of symbol indicating the specimen's (a) length, (b) width, and (c) form. For (b) and (c), $n = 155$.

Figure 4. Scatterplots of the form f against the ratio $r_{sh} = \sigma_{xx}/\sigma_{yy}$ for (a) the L subsample (with regression line shown) and (b) the combined C, A, W, and S subsamples (less two specimens with $r_{sh} > 50$). Clusters A and B in (a) are of ladybirds and lacewings respectively; regions C, D, and E are occupied by carabid beetles, hoverflies, and moths respectively. Specimens with $m \leq 80$ mg in (b) are marked with a +.

Figure 5. Positions on the (α_2, α_4) plane of CLPP dataset specimens in different mass ranges. The symbols indicate the specimens' forms f (see key at top left).

Figure 6. Schematic trajectory on the (α_2, α_4) plane traced by a notional 'typical insect' as its mass increases (grey line). The ellipses show the approximate area of the plane occupied by CLPP specimens for each of the mass ranges of Figure 5 (with the two similar distributions for $70 < m < 100$ mg and $100 < m < 150$ mg combined, and see Table 6); they provide an indication of the lateral spread of points from the notional trajectory line. The dashed lines are contours of $r_{sh} = \sigma_{xx}/\sigma_{yy}$ with values 2, 5, 10, and 20.
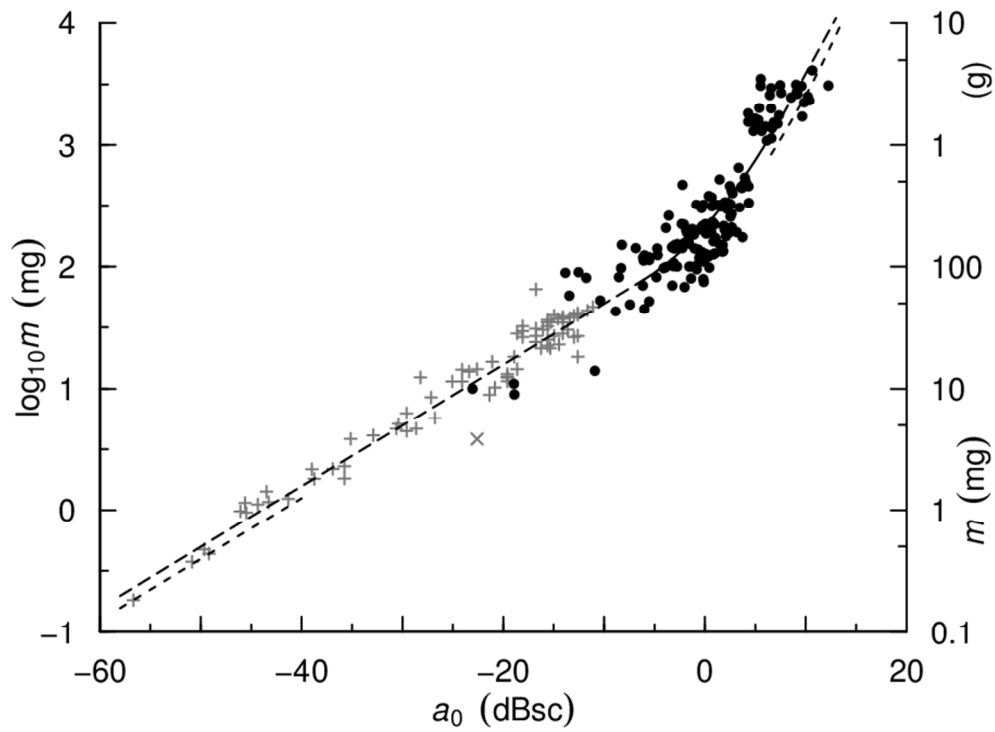
Figure 1
Insert Figure 1 near here
325x238mm (72 x 72 DPI)

Figure 2
Insert Figure 2 near here
130x88mm (300 x 300 DPI)

Figure 3
Insert Figure 3 near here
195x199mm (300 x 300 DPI)

Figure 4
Insert Figure 4 near here
77x32mm (300 x 300 DPI)

1
2
3
4
5
6
7
8
9
10
11
12
13
14
15
16
17
18
19
20
21
22
23
24
25
26
27
28
29
30
31
32
33
34
35
36
37
38
39
40
41
42
43
44
45
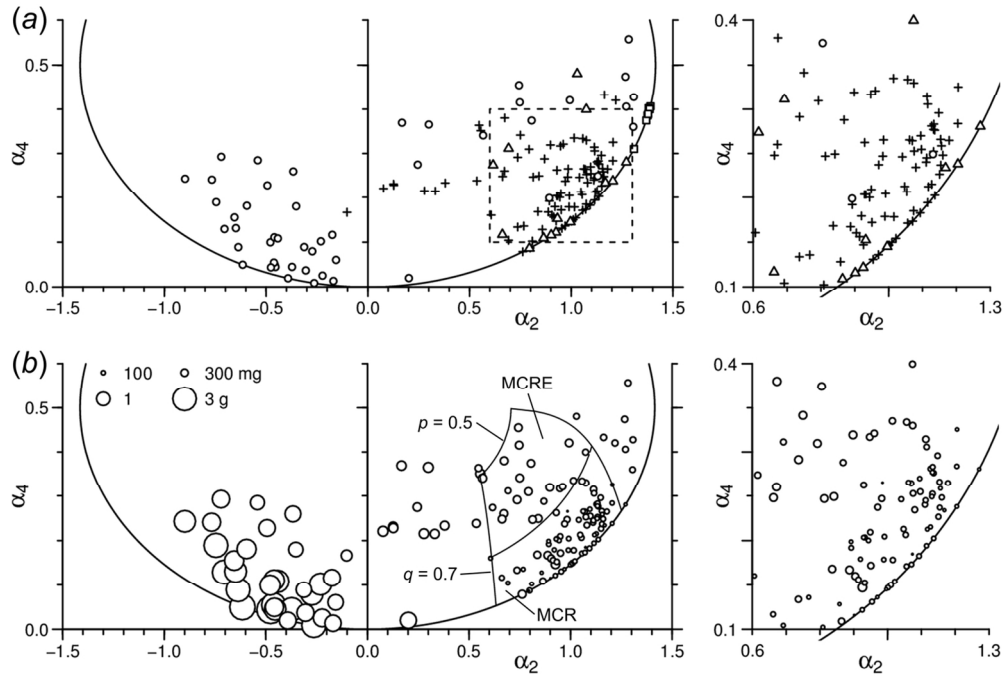46
47
48
49
50
51
52
53
54
55
56
57
58
59
60

Figure 5
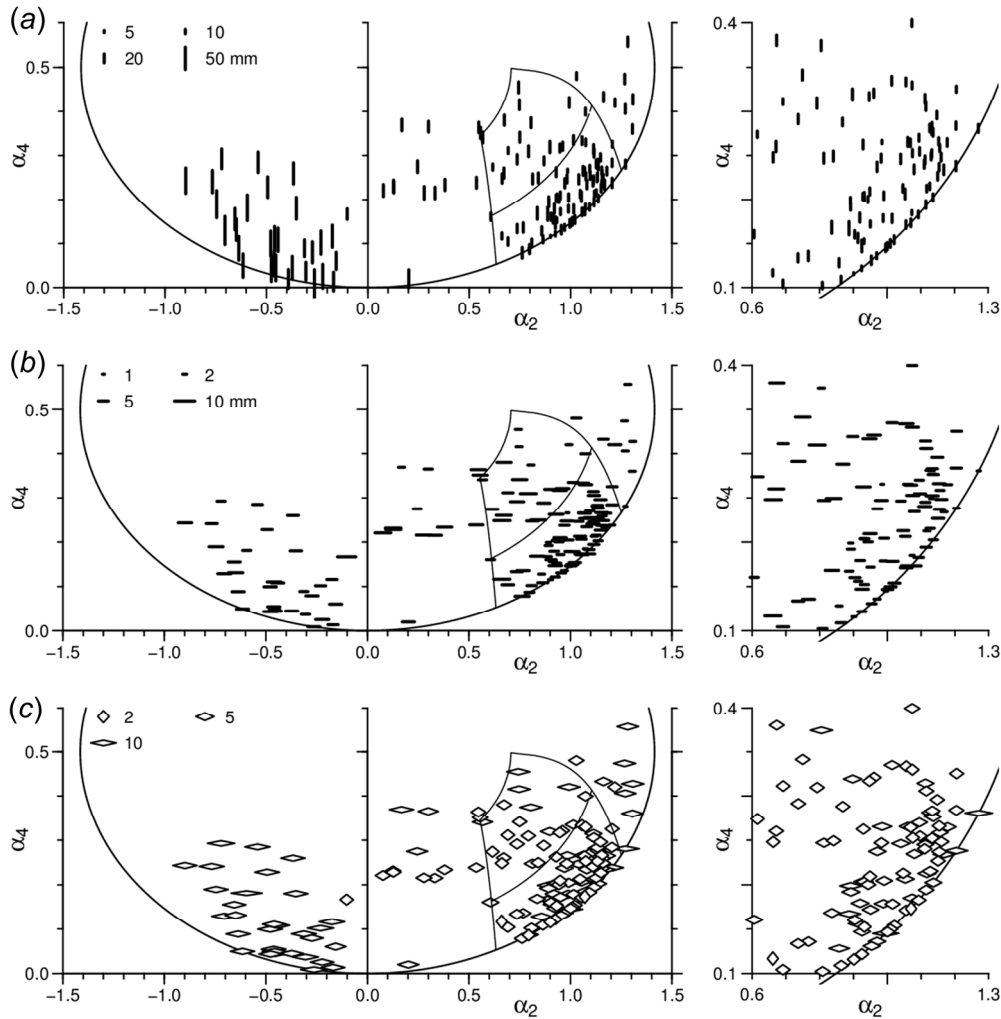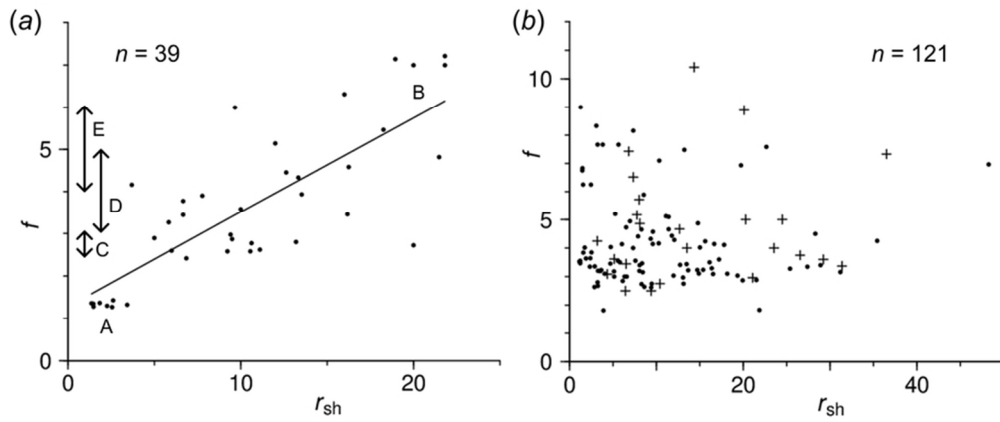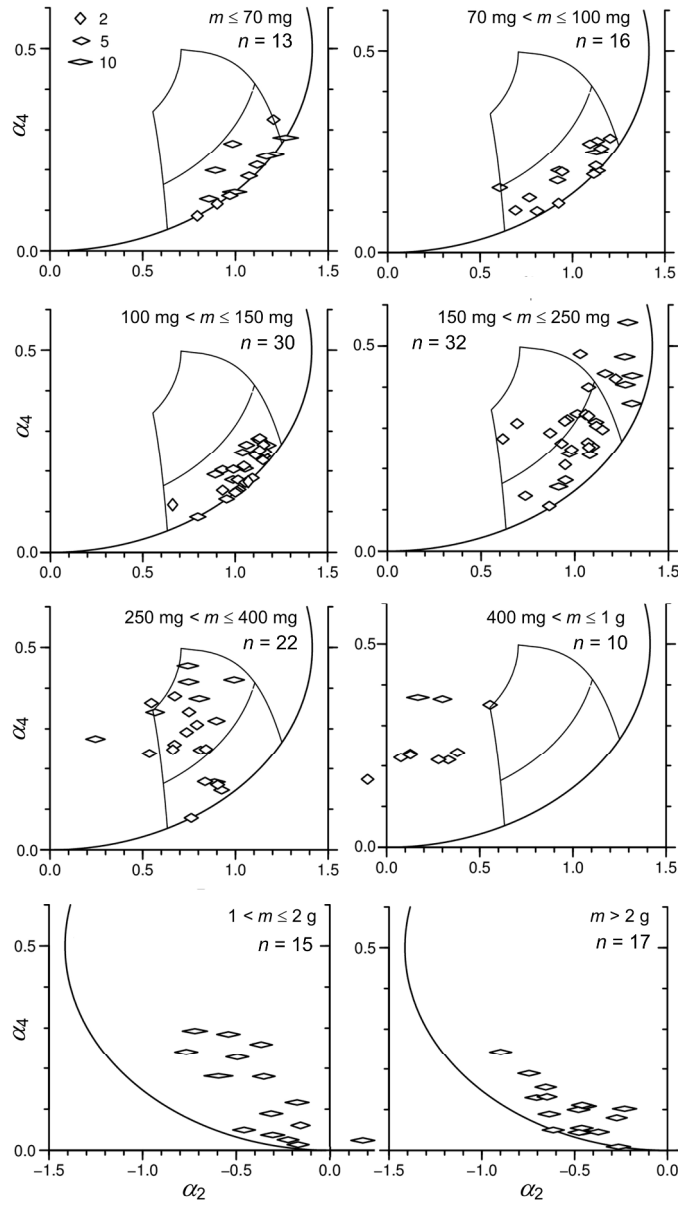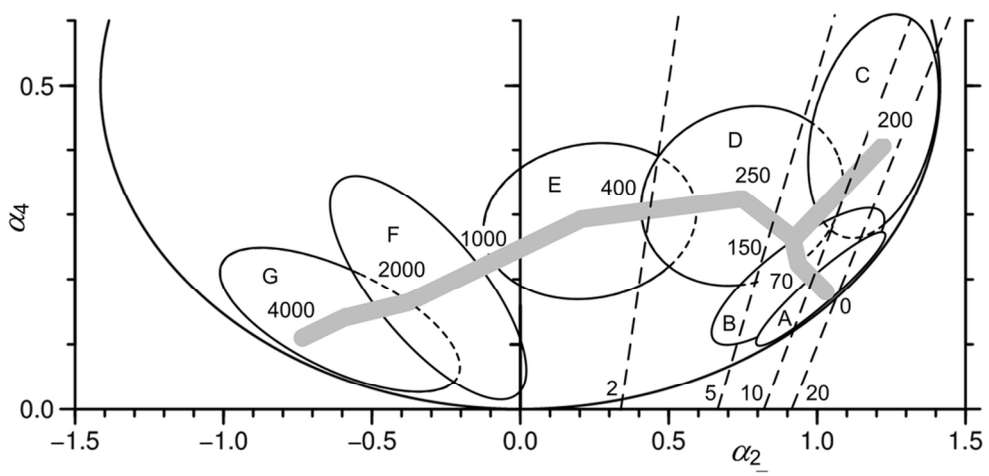Insert Figure 5 near here
238x412mm (300 x 300 DPI)

Figure 6
Insert Figure 6 near here
93x43mm (300 x 300 DPI)